The Conserved Active-Site Loop Residues of Ferrochelatase Induce Porphyrin Conformational Changes Necessary for Catalysis†

Zhen Shi,‡ Ricardo Franco,§ Raid Haddad,||,⊥ John A. Shelnutt,*,⊥,@ and Gloria C. Ferreira*,‡,#

Department of Biochemistry and Molecular Biology, College of Medicine, and H. Lee Moffitt Cancer Center and Research Institute, University of South Florida, Tampa, Florida 33612-4799, REQUIMTE, Departamento de Química, Faculdade de Ciências e Tecnologia, Universidade Nova de Lisboa, 2829-516 Caparica, Portugal, Department of Chemical and Nuclear Engineering, University of New Mexico, Albuquerque, New Mexico 87131, Surface and Interface Sciences Department, Sandia National Laboratories, Albuquerque, New Mexico 87185-1349, and Department of Chemistry, University of Georgia, Athens, Georgia 30602-2556

Received September 19, 2005; Revised Manuscript Received December 7, 2005

ABSTRACT: Binding of porphyrin to murine ferrochelatase, the terminal enzyme of the heme biosynthetic pathway, is investigated by employing a set of variants harboring mutations in a putative porphyrin-binding loop. Using resonance Raman (RR) spectroscopy, the structural properties of the ferrochelatase-bound porphyrins are examined, especially with respect to the porphyrin deformation occurring in the environment of the active site. This deformation is thought to be a key step in the enzymatic insertion of ferrous iron into the porphyrin ring to make heme. Our previous RR spectroscopic studies of binding of porphyrin to murine ferrochelatase led us to propose that the wild-type enzyme induces porphyrin distortion even in the absence of the metal ion substrate. Here, we broaden this view by presenting evidence that the degree of a specific nonplanar porphyrin deformation contributes to the catalytic efficiency of ferrochelatase and its variants. The results also suggest that the conserved Trp256 (murine ferrochelatase numbering) is partially responsible for the observed porphyrin deformation. Binding of porphyrin to the ferrochelatase variants causes a decrease in the intensity of RR out-of-plane vibrational mode γ_{15}, a saddling-like mode that is strong in the wild-type enzyme. In particular, the variant with a catalytic efficiency 1 order of magnitude lower than that of the wild-type enzyme is estimated to produce less than 30% of the wild-type saddling deformation. These results suggest that specific conserved loop residues (especially Trp256) are directly involved in the saddling of the porphyrin substrate.

The terminal step in heme biosynthesis is catalyzed by ferrochelatase (EC 4.99.1.1, protoheme ferrolyase), which inserts ferrous iron into protoporphyrin IX to produce protoheme (*1*−*3*). Identified in a large number of organisms, ferrochelatase exhibits a folding pattern and an active-site structure with a high degree of homology across taxa (*1*, *2*). As shown in the X-ray crystal structures of the enzyme from *Bacillus subtilis* (*4*, *5*), human (*6*), and *Saccharomyces cerevisiae* (*7*), the monomeric unit consists of two domains, each with a Rossmann-type fold. Porphyrin binds to a deep cleft between the two domains (*5*), which is rich in conserved residues proposed to be important in metal and porphyrin binding and catalysis (*7*, *8*).

The most widely accepted reaction mechanism for ferrochelatase suggests that a critical step involves distortion of the porphyrin macrocycle which exposes the lone-pair orbitals of the pyrrole nitrogens to the incoming metal ion (*9*). This notion has received support from both experimental and theoretical studies (*5*, *10*−*12*) which show that an out-of-plane distortion occurs upon substrate binding. The X-ray structure of the strong complex between bacterial ferrochelatase and the substrate analogue *N*-methylmesoporphyrin showed deformation of the macrocycle, including tilting of pyrrole ring A and distortion of the other pyrroles to yield a predominantly saddled−ruffled structure (*5*). Although this porphyrin conformation would necessarily result from the *N*-methyl substitution, the high affinity of the protein for porphyrin locked into this conformation suggests that it corresponds to a preferred porphyrin structure in the active site. Moreover, antibodies raised against nonplanar alkylated porphyrins were found to catalyze porphyrin metalation by Zn^{2+} and Cu^{2+} (*12*). Resonance Raman (RR)[1] spectra of the antibody-bound mesoporphyrin revealed an out-of-plane distortion (*10*), and the X-ray structure of the Michaelis

† This work was supported by American Cancer Society Grant RSG-96-05106-TBE to G.C.F. Sandia National Laboratories is a multiprogram laboratory operated by Sandia Corp., a Lockheed Martin company, for the U.S. Department of Energy under Contract DE-AC04-94AL85000.

* To whom correspondence should be addressed. G.C.F.: Department of Biochemistry and Molecular Biology, College of Medicine, MDC 7, University of South Florida, Tampa, FL 33612-4799; telephone, (813) 974-5797; fax, (813) 974-0504; e-mail, gferreir@hsc.usf.edu. J.A.S.: Sandia National Laboratories, Albuquerque, NM 87185-1349; telephone, (505) 272-7160; fax, (505) 272-7077; e-mail, jasheln@unm.edu.

‡ Department of Biochemistry and Molecular Biology, College of Medicine, University of South Florida.

§ Universidade Nova de Lisboa.

|| University of New Mexico.

⊥ Sandia National Laboratories, Albuquerque.

@ University of Georgia.

H. Lee Moffitt Cancer Center and Research Institute, University of South Florida.

10.1021/bi051907i CCC: $33.50
Published on Web 02/07/2006

```
  1  TTKPQAQPER RKPKTGILML NMGGPETLGE VQDFLQRLFL DRDLMTLPIQ NKLAPFIAKR
 61  RTPKIQEQYR RIGGGSPIKM WTSKQGEGMV KLLDELSPAT APHKYYIGFR YVHPLTEEAI
121  EEMERDGLER AIAFTQYPQY SCSTTGSSLN AIYRYYNEVG QKPTMKWSTI DRWPTHPLLI
181  QCFADHILKE LNHFPEEKRS EVVILFSAHS LPMSVVNRGD PYPQEVGATV HKVMEKLGYP
241  NPYRLVW***QSK VGPVPWL***GPQ TDEAIKGLCE RGRKNILLVP IAFTSDHIET LYELDIEYSQ
301  VLAQKCGAEN IRRAESLNGN PLFSKALADL VHSHIQSNKL CSTQLSLNCP LCVNPVCRKT
361  KSFFTSQQL
```

FIGURE 1: Amino acid sequence for the mature form of murine ferrochelatase. The porphyrin-binding loop motif is in italics and bold font and underlined. The numbering of amino acids is according to the mouse genome sequence submitted by the Genome Exploration Research Group in RIKEN, Japan (GenBank nucleotide accession number AK004718.2), and sequencing results in our laboratory (*18*). In the previously deposited sequence (GenBank protein accession number AAA80530), two codons (i.e., for Q68 and Y69) were omitted.

complex of the catalytic antibody bound to substrate mesoporphyrin in the absence of metal ions demonstrated an out-of-plane macrocycle distortion with saddling, ruffling, and some doming deformations (*13*). These results thus substantiate the idea that the porphyrin distortion induced by the antibody resembles that induced by alkylation and that this leads to ferrochelatase activity (*10*, *13*). Indeed, this assertion was recently "quantified" with the observation that the activation of the Raman band assigned to γ_{15} (an out-of-plane porphyrin vibration) could be directly related to the degree of affinity maturation of the catalytic antibody (*14*).

Further support for this mechanism comes from different theoretical methods (e.g., combined quantum mechanical and molecular mechanics calculations) used to calculate the energetics associated with porphyrin distortion, especially the porphyrin distortion found in the porphyrin−ferrochelatase complex. These calculations established the significance of the nonplanar deformation of the porphyrin substrate in relation to the ferrochelatase-catalyzed reaction (*15*). In addition to exposure of the pyrrole nitrogens to the incoming metal ion, two favorable consequences were evident. (1) A pK_a decrease of the two protonated pyrrole rings promotes the reaction because deprotonation has to occur before metal insertion, and (2) product release may be facilitated because metalloporphyrins are harder to distort than the free-base porphyrin and thus have lower affinity for the active site (*15*).

It has been shown that wild-type murine ferrochelatase can induce porphyrin distortion even without the binding of the ferrous iron substrate (*16*, *17*). In these studies, the specificity of porphyrin binding was demonstrated by monitoring the titration of ferrochelatase with porphyrin at substoichiometric porphyrin:protein ratios using RR spectroscopy. This facilitates observation of the vibrational modes of the fraction of bound porphyrins and, in particular, reveals frequency shifts in the Raman structure-sensitive lines of the bound porphyrins that are obscured by the unbound porphyrin present at stoichiometric ratios (*17*). Of special interest is γ_{15}, a B_{2u} symmetry (saddling-like) out-of-plane mode, which was observed in the RR spectrum of free-base protoporphyrin bound to wild-type ferrochelatase (*17*). Out-of-plane modes of a particular symmetry gain intensity from the corresponding symmetric deformation of the porphyrin. Significantly, saddling is a B_{2u} (D_{4h} classification) out-of-plane deformation that exposes both the protons and the lone pairs of the nitrogen atoms of the porphyrin core; thus, it is a porphyrin deformation suitable for promoting metal insertion by ferrochelatase.

Molecular mechanics simulations led to the original proposal that a highly conserved sequence [Gln248−Leu257, murine ferrochelatase numbering (Figure 1)] forms a loop (*16*) that is involved in porphyrin binding. With the determination of the ferrochelatase X-ray structure (*6*, *7*), this loop was subsequently confirmed to be in the active-site cleft. Strikingly, the active-site loop can accommodate multiple functional substitutions (*18*). However, certain amino acids within the loop exhibit a high informational content as evidenced by the limited number of tolerated substitutions in these positions (*18*). Further, kinetic analysis of selected active variants suggested that the loop mutations resulted in a general disruption of the interaction between the porphyrin substrate and ferrochelatase (*18*).

In this study using RR spectroscopy, we examine the effects of these amino acid substitutions on porphyrin distortion and provide a detailed characterization of the involvement of some of the loop residues in porphyrin distortion and ferrochelatase catalysis. Most significantly, we observe that weakened induction of the saddled deformation upon binding of porphyrin to the ferrochelatase variants is related to reduced catalytic efficiencies of the variants relative to that of the wild-type enzyme. Trp256 plays a crucial role in the porphyrin distortion. Additionally, several loop variants exhibit alterations in the vibrational modes that are associated with the porphyrin vinyl and propionate groups, which suggest that reorientation and/or relocation of the porphyrin side chains may also occur in the mutated active sites. These RR studies begin to establish the role of the active-site loop in binding of porphyrin to ferrochelatase and porphyrin distortion during catalysis.

MATERIALS AND METHODS

Materials. Protoporphyrin IX and Ni(II) protoporphyrin were from Frontier Scientific, while hemin was from Sigma Chemicals. Porphyrins were used without further purification. Polyethylene glycol sorbitan monooleate (Tween 80), tris(hydroxymethyl)aminomethane carbonate (Trizma base), bovine serum albumin, and the bicinchonic acid protein determination reagents were from Sigma Chemicals. HPLC-grade H_2O was from Fisher Scientific. Reagents for sodium

[1] Abbreviations: hemin, iron(III) protoporphyrin IX; NiPP, Ni(II) protoporphyrin IX; *N*-MMP, *N*-methylmesoporphyrin; H_2PP, free-base protoporphyrin IX; RR, resonance Raman.

Table 1: Results of the Spectral Simulations for Protein-Bound Free-Base Protoporphyrin Based on Least-Squares Fitting with Lorentzian Line Shapes and a Fixed Width (2.814 cm^{-1}) for the γ_{15} Line[a]

protein	ν_7 (cm^{-1})	intensity (area)	total intensity (area)	γ_{15} (cm^{-1})	total intensity (area)	relative intensity (γ_{15}/ν_7)	% of wild-type relative intensity[b]	K_m^{PP} (μM)	k_{cat}/K_m^{PP} (min^{-1} μM^{-1})
wild-type	673.3	1624.5							
ferrochelatase	678.0	1408.8	3033.3	700.4	455.8	0.150	100.0	1.40 ± 0.20[c]	2.93[c]
P255R	674.3	1059.6							
	679.0	745.6	1805.2	701.0	244.4	0.135	90.1	2.65 ± 0.44[c]	2.94[c]
S249A/K250Q/V251C	673.8	2166.5							
	678.5	1517.9	3684.4	700.8	481.8	0.131	87.0	6.84 ± 1.74[c]	2.63[c]
P255G	675.3	1752.3							
	682.7	514.4	2266.7	700.6	126.0	0.056	37.0	2.51 ± 0.80	2.35
Q248P/S249G/K250P/G252W	674.9	6632.7							
	679.8	2349.2	8981.9	701.0	1088.9	0.121	80.7	10.34 ± 1.14[c]	1.36[c]
K250M/V251L/W256Y	676.8	3124.6							
	685.5	531.9	3656.5	701.3	158.6	0.043	28.8	11.25 ± 2.45[c]	0.27[c]

[a] Variant proteins are ordered in the table by decreasing catalytic efficiency (k_{cat}/K_m^{PP}). [b] The % of wild-type relative intensity was determined by normalizing the relative intensity (γ_{15}/ν_7) corresponding to each variant against that of the wild-type ferrochelatase. [c] From ref *18*.

dodecyl sulfate−polyacrylamide gel electrophoresis were from Bio-Rad Laboratories. Superdex-200 gel filtration matrix was from Amersham Biosciences. Talon metal chelate affinity resins were from BD Biosciences. All reagents were of the highest purity available.

Protein Purification. The wild-type murine ferrochelatase and the ferrochelatase loop variants were expressed under the *Escherichia coli* alkaline phosphatase promoter *phoA* as described previously (*19*). The recombinant proteins containing a N-terminal pentahistidine tag were purified from wild-type ferrochelatase- or variant-hyperproducing BL21(DE3) cells using a previously described protocol (*16*) with some modifications (*18*). The wild-type ferrochelatase was derived from the pGF47 expression plasmid (*16*), while the loop variants were obtained from plasmids harboring functional substitutions selected from a library constructed by random mutagenesis of the loop motif (*18*).

Aliquots of 200 μL of purified concentrated proteins (typically at 100−150 μM) in EQ buffer [20 mM Tris-HCl (pH 8), 10% glycerol, and 150 mM NaCl] were stored in liquid N_2 until they were used. Protein purity was assessed by sodium dodecyl sulfate−polyacrylamide gel electrophoresis (*20*), and protein concentrations were determined using the bicinchoninic acid assay (*21*) with bovine serum albumin as the standard.

Porphyrin Solutions. Stock solutions were prepared by dissolving porphyrin in 100 μL of 2 N NH_4OH and then adding 100 μL of 10% (v/v) Tween 80 and 1.8 mL of H_2O. Typically, stocks were made as 2 mM solutions and further diluted in EQ buffer before the Raman spectra were collected.

Resonance Raman Spectroscopy. Samples for RR spectra were prepared by mixing porphyrins (typically 6 μM) and proteins (typically 60 μM) in EQ buffer. The final concentration of detergent, i.e., Tween 80, was adjusted to 12 μM. The samples, in a final volume of ~100 μL, were transferred into a stoppered 3 mm × 3 mm cross-section optical cell (NSG Precision Cells). Raman samples were kept on ice until the collection of spectra. Typically, the spectra were taken at room temperature (26 °C) for 2−10 min using 20 mW of laser power. The spectra were obtained using the 406.7 nm line of an INNOVA 304 Kr^+ laser (Coherent) and using a Raman spectrometer as previously described (*17*). Briefly, the spectrometer was a 0.75 m monochromator with a 2048-channel liquid N_2-cooled CCD detector (Instruments, SA). Position mode was used for CCD detection, with each section covering ~500 cm^{-1} of the Raman spectrum without moving the grating.

The RR spectra were exported as even-X ASCII files for plotting with SigmaPlot (SPSS). Lorentzian decomposition of the spectra was performed using PeakFit (SYSTAT). Curve fitting was used to obtain the frequencies for the centers of the structure-sensitive lines. For the region near saddling symmetry (B_{2u}) mode γ_{15}, the spectral fitting procedure was adjusted to take into account the varying signal:noise characteristics of the low-frequency RR spectra for binding of free-base porphyrin to the proteins. First, the spectra of porphyrin bound to wild-type ferrochelatase and the quadruple mutant Q248P/S249G/K250P/G252W, which exhibited the highest signal:noise ratio, were fit with all parameters free, including the center, width, and amplitude of each Lorentzian band, as well as the slope and intercept of a linear baseline. Eight lines were used to fit the frequency region from 580 to 780 cm^{-1}, and the average half-width at half-maximum of γ_{15} was determined to be 2.814 cm^{-1}. This value for the width was then fixed, and the data were refit. These parameters were used for the constrained fits, and the results are reported in Table 1.

Enzymatic Activity Assay. Ferrochelatase activity was determined by monitoring the consumption of substrate protoporphyrin using ferrous iron as the metal substrate in a continuous spectrofluorimetric assay conducted under strictly anaerobic conditions as described previously (*22*). The steady-state kinetic parameters for the wild-type enzyme and loop variants were determined by fitting data to the Michaelis−Menten equation as described previously (*18*).

RESULTS

Binding of H_2PP to Porphyrin-Binding Loop Variants of Ferrochelatase. Substrate (i.e., free-base protoporphyrin IX) binding at the active site of ferrochelatase variants was assessed for a H_2PP:protein molar ratio of 0.1 using RR spectroscopy in a fashion similar to that previously devised for wild-type murine ferrochelatase (*17*). Figure 2 illustrates the low-frequency (Figure 2A) and high-frequency (Figure 2B) regions of the RR spectra of H_2PP incubated with the ferrochelatase variants at a porphyrin:protein molar ratio of

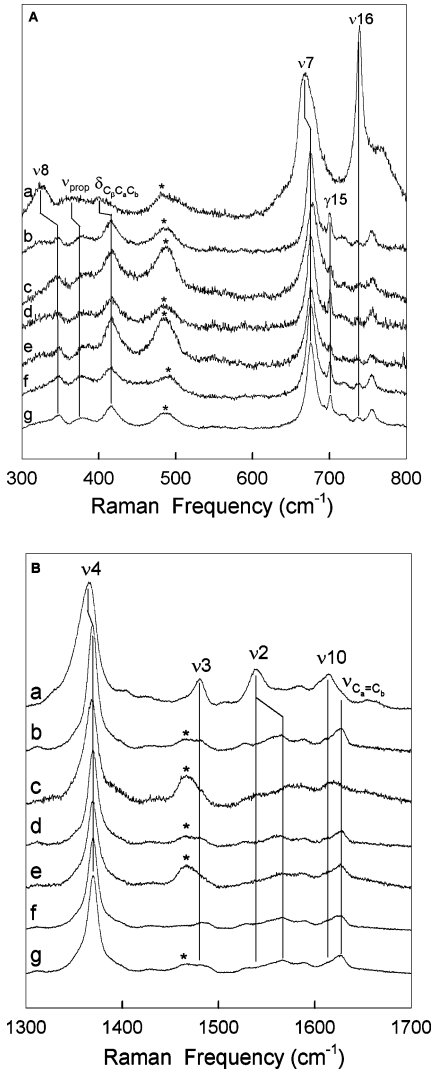

FIGURE 2: Low-frequency (A) and high-frequency (B) regions of the resonance Raman spectra of H_2PP in assay buffer (a) or bound to wild-type ferrochelatase (b) and to porphyrin-binding loop variants (c−g) after incubation with a H_2PP:protein molar ratio of 0.1: (c) triple mutant K250M/V251L/W256Y, (d) single mutant P255R, (e) single mutant P255G, (f) triple mutant S249A/K250Q/V251C, and (g) quadruple mutant Q248P/S249G/K250P/G252W. Asterisks denote buffer lines. Vibrational modes of the major structure-sensitive lines are labeled.

0.1 (Figure 2, c−g). The RR spectra of H_2PP in assay buffer (Figure 2, spectrum a) and H_2PP incubated with wild-type ferrochelatase (Figure 2, spectrum b) are given for comparison. There are clear differences in the RR spectra of porphyrin bound to ferrochelatase variants when compared to those of the porphyrin in the detergent micellar environment. Specifically, in the low-frequency region (Figure 2A), as was found for wild-type ferrochelatase (ref *17* and Figure 2A, spectrum b), the ν_7 line upshifted from 666 cm^{-1} for porphyrin in the assay buffer to 673−675 cm^{-1} in four of the variants (Figure 2A, spectra d−g); the largest shift (to 677 cm^{-1}) was detected in the porphyrin bound to the triple mutant K250M/V251L/W256Y (Figure 2A, spectrum c). The ν_{16} line [at 738 cm^{-1} for unbound H_2PP in solution (Figure 2A, spectrum a)] decreased in intensity and frequency for wild-type ferrochelatase-bound porphyrin and four variant-bound species (Figure 2A, spectra b and d−g), whereas the ν_{16} line for the triple mutant K250M/V251L/W256Y-bound porphyrin shifted to a higher frequency, albeit with diminished intensity (Figure 2A, spectrum c). Importantly, comparison of the spectra of free-base porphyrin, incubated with either wild-type ferrochelatase or ferrochelatase variants (Figure 2A, spectra b−g), with that of free-base porphyrin in assay buffer (Figure 2A, spectrum a) showed that a strong γ_{15} mode was activated upon protein binding.

RR spectra in the high-frequency region (Figure 2B) also exhibited distinct differences between H_2PP bound to the variants or wild-type ferrochelatase and free H_2PP. The ν_2 line was considerably reduced in intensity for porphyrin bound both to the wild-type enzyme and to the variants (Figure 2B, spectra b−g) when compared to the porphyrin in assay buffer (Figure 2B, spectrum a); in particular, the ν_2 line upshifted by an additional 5 cm^{-1} in porphyrin bound to the triple mutant K250M/V251L/W256Y relative to that of the wild-type protein (Figure 2B, spectra b and c). In fact, the shift induced in ν_2 of H_2PP by this variant was the greatest observed when all variants were considered and reflected important changes in the interaction of the vinyl group with the protein (Figure 2B, spectra b−g). Further, protein binding led to sharpening of the $\nu_{Ca=Cb}$ vinyl stretching mode of H_2PP in wild-type ferrochelatase and variants (Figure 2B). While the frequency of the $\nu_{Ca=Cb}$ line remained unchanged for porphyrin bound to the wild-type protein and four variants (Figure 2B, spectra b and d−g), the $\nu_{Ca=Cb}$ band was broadened and downshifted in the variant K250M/V251L/W256Y-bound species (Figure 2B, spectrum c), again implicating disruption of the interaction of the vinyl group with the protein.

Binding of NiPP to Porphyrin-Binding Loop Variants of Ferrochelatase. Our previous RR studies indicated that NiPP became distorted from planarity upon binding to wild-type ferrochelatase (*17*). NiPP shows a strong tendency to distort in a way that allows the porphyrin to contract around the small Ni(II) ion, making it a sensitive probe of the active site. We examined the binding of this metalloporphyrin to the loop variants to assess the impact of the introduced mutations on metalloporphyrin deformation. Figure 3 depicts the low-frequency (Figure 3A) and high-frequency (Figure 3B) regions of the RR spectra of NiPP in assay buffer (Figure 3, spectrum a), NiPP incubated with wild-type ferrochelatase (Figure 3, spectrum b), and NiPP incubated with loop variants (Figure 3, spectra c−g). The addition of NiPP to both wild-type ferrochelatase and the porphyrin-binding loop variants resulted in a sharpening of the RR lines of the bound porphyrin in the high-frequency region of the spectra (Figure 3B, spectra b−g) in relation to those of NiPP in assay buffer (Figure 3B, spectrum a). Also, upon protein binding, the ν_2, ν_3, and ν_{10} structure-sensitive lines downshifted, while the vinyl stretching mode ($\nu_{Ca=Cb}$) sharpened and increased in intensity (Figure 3B, spectra b−g) as previously found for wild-type ferrochelatase (*17*). Compared with that of NiPP bound to the wild-type protein (Figure 3A, spectrum b), the low-frequency region of the RR spectra of both triple mutants, K250M/V251L/W256Y (Figure 3A, spectrum c) and S249A/K250Q/V251C (Figure 3A, spectrum f), exhibited a less pronounced splitting of the ν_7 lines and broader propionate lines. Also, the ν_8 line, which downshifts and splits for wild-type ferrochelatase and all other mutants, presents a spectral structure for both triple mutants (Figure 3A, spectra c and f) that is similar to that of the unbound

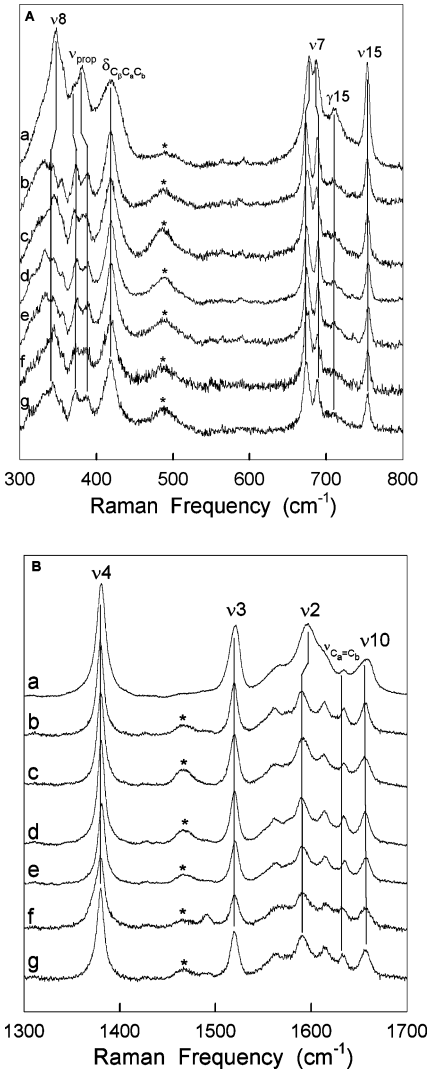

FIGURE 3: Low-frequency (A) and high-frequency (B) regions of the resonance Raman spectra of NiPP in assay buffer (a) or bound to wild-type ferrochelatase (b) and to porphyrin-binding loop variants (c−g) after incubation with a NiPP:protein molar ratio of 0.1: (c) triple mutant K250M/V251L/W256Y, (d) single mutant P255R, (e) single mutant P255G, (f) triple mutant S249A/K250Q/V251C, and (g) quadruple mutant Q248P/S249G/K250P/G252W. Asterisks denote buffer lines.

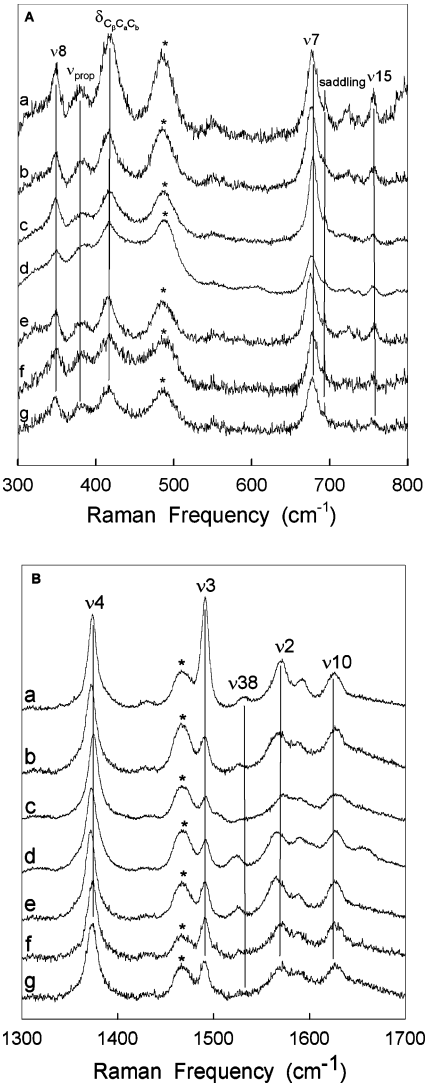

FIGURE 4: Low-frequency (A) and high-frequency (B) regions of the resonance Raman spectra of hemin in assay buffer (a) or bound to wild-type ferrochelatase (b) and to porphyrin-binding loop variants (c−g) after incubation with a hemin:protein molar ratio of 0.1: (c) triple mutant K250M/V251L/W256Y, (d) single mutant P255R, (e) single mutant P255G, (f) triple mutant S249A/K250Q/V251C, and (g) quadruple mutant Q248P/S249G/K250P/G252W. Asterisks denote buffer lines.

NiPP in assay buffer. These alterations in the RR spectra of variant-bound NiPP make these spectra resemble more closely the RR spectrum of the unbound NiPP in assay buffer (Figure 3A, spectrum a) rather than that of NiPP bound to wild-type ferrochelatase (Figure 3A, spectrum b). This suggests that, in relation to the wild-type enzyme, the triply mutated variants have lower affinities for NiPP and a looser interaction with the porphyrin (see Discussion).

Binding of Hemin to Porphyrin-Binding Loop Variants of Ferrochelatase. The interaction of the loop variants with hemin, an inhibitor of ferrochelatase (*23*), was examined by collecting RR spectra of hemin upon incubation with the variants and comparing these spectra against those of free hemin in assay buffer and hemin bound to wild-type ferrochelatase (Figure 4). Binding of hemin to both Pro255 variants resulted in a shift of the ν_2 line to lower frequencies, with a magnitude of 5 cm^{-1} for P255R (Figure 4B, spectrum d) and 4.2 cm^{-1} for P255G (Figure 4B, spectrum e), whereas all other variants exhibited smaller (typically 1.5 cm^{-1}) shifts in the opposite direction, i.e., to higher frequencies (Figure 4B, spectra c, f, and g). The ν_{38} line, associated with $C_\beta-C_\beta$ and $C_\beta-C_1$ stretches, increased in intensity in the cases of P255R and P255G as compared to that of the wild-type protein, although it did not appreciably shift (Figure 4B, spectra b, d, and e). Both the ν_2 and ν_{38} lines derived from vinyl-associated modes, so the fact that they changed in tandem indicates significant alterations in the vinyl groups of the variant-bound porphyrins.

In the low-frequency region of the RR spectra of the wild-type and variant-bound hemin, two different types of spectra can be distinguished: the wild-type, P255R, and P255G enzyme spectra all exhibit similar characteristics (Figure 4A, spectra b, d, and e), namely, a downshifted ν_7 and downshifted vinyl bending lines ($C_\beta C_a C_b$) in relation to the free hemin in assay buffer. The second type of spectrum is represented by the triple and quadruple variants that exhibit

RR spectra (Figure 4A, spectra c, f, and g) very similar to that of free hemin in assay buffer (Figure 4A, spectrum a).

DISCUSSION

As reported previously (*18*), replacement of the residues in an active-site loop disrupted the interaction between ferrochelatase and bound porphyrin. The K_m values for protoporphyrin for a set of loop variants were increased 2−8-fold relative to that of wild-type ferrochelatase (*18*). Although these increased K_m values were associated with decreased catalytic efficiencies (k_{cat}/K_m^{PP}), the k_{cat} values were not always lower than the wild-type value (*18*). The most dramatic effect on the steady-state kinetic parameters was introduced with the triple K250M/V251L/W256Y mutations. This variant exhibited a 1 order of magnitude lower k_{cat}/K_m^{PP} than the wild-type enzyme, due to a much compromised porphyrin binding, as indicated by an 8-fold increase in K_m^{PP} and an ∼30% decrease in k_{cat} (*18*). In this study, we have presented an in-depth analysis of the parameters affecting porphyrin binding, distortion, and catalysis of the ferrochelatase porphyrin-binding loop variants.

Nonplanar Porphyrin Distortion and Catalytic Efficiency. Analysis of the high-frequency RR spectra of wild-type murine ferrochelatase and its active-site loop variants with H_2PP bound led us to conclude that the protein is responsible for inducing important distortions in the porphyrin macrocycle. Saddling of H_2PP occurs upon its binding to the active-site pocket of the variants, as previously observed for wild-type ferrochelatase (*17*). Significantly, the extent of substrate saddling influences the catalytic efficiency of the enzyme toward H_2PP. The γ_{15} mode, a B_{2u} symmetry saddling-like mode, was previously observed, and its appearance was attributed to a saddling deformation of the porphyrin upon binding to the protein (*17*, *24*). Although all of the RR spectra of the analyzed variants and wild-type ferrochelatase exhibited strong γ_{15} lines relative to those of H_2PP in buffer, their intensities varied among the different variants (Figure 2A). The integrated intensity of the γ_{15} line, normalized to the intensity of the ν_7 line for the same spectrum, can be taken as a measure of the degree of porphyrin saddling deformation induced by the different proteins (*14*). Table 1 lists values for the ratio of the intensities of γ_{15} and ν_7 lines and values for the catalytic efficiencies, measured by the ratio between the k_{cat} of the enzymatic reaction and the K_m for H_2PP under steady-state turnover conditions for the wild-type and loop ferrochelatase variants. The degree of saddling-type distortion as measured by the relative intensity of the γ_{15} line (γ_{15}/ν_7) is high when the catalytic efficiency of the variants is near that of the wild-type enzyme. In contrast, the binding of H_2PP to the triple mutant K250M/V251L/W256Y produced the smallest saddling of the porphyrin macrocycle (as determined from γ_{15}/ν_7) among all of the examined variants: the saddled deformation is less than 30% of that of the wild-type (Table 1), and strikingly, the catalytic efficiency (k_{cat}/K_m) of K250M/V251L/W256Y is lowered by 1 order of magnitude (*18*). These data are consistent with the previously proposed key role for the porphyrin saddling deformation in the enzyme catalytic mechanism.

The catalytic efficiency of the ferrochelatase loop variants also exhibited an approximate inverse linear correlation with the frequency of the ν_7 line of bound H_2PP (see Table 1); that is, a larger ν_7 line frequency is associated with a lower catalytic efficiency (k_{cat}/K_m^{PP}) of the variant, and the lowest frequency is associated with the wild-type protein. The ν_7 line corresponds to an A_{1g} in-plane pyrrole ring symmetric deformation (*17*, *25*); such an in-plane deformation might be expected to accompany the saddling and other deformations that occur upon porphyrin binding. This is especially true for saddling, which contracts the core of the porphyrin ring. However, in-plane deformations are not expected to influence catalytic efficiency as much as the out-of-plane deformations which expose the nitrogens.

Analysis of the steady-state kinetic parameters in relation to porphyrin saddling among the ferrochelatase variants indicated an approximate inverse relationship of K_m^{PP} with the extent of saddling (Table 1). For P255R, S249A/K250Q/V251C, and Q248P/S249G/K250P/G252W variants, the increasingly poor interaction with protoporphyrin was accompanied by a gradual reduction in the level of porphyrin saddling, reaching values of ∼80% of the wild-type level. However, while the K_m^{PP} increase for the K250M/V251L/W256Y variant was similar to that of the Q248P/S249G/K250P/G252W variant, the level of induced porphyrin saddling was only ∼30% of that imposed by the wild-type protein; this indicates a marked deficiency in the capacity of the K250M/V251L/W256Y variant to distort porphyrin, which may not be related solely to the effect on K_m^{PP}. Therefore, it is likely that multiple factors can influence the competency of ferrochelatase to distort the porphyrin. A maximal degree of distortion may require the optimal active-site geometry. Alteration of the active-site residues in the variants that were examined causes alterations of the porphyrin-binding cavity structure (*18*), and as a result, it may have become unfavorable for inducing the porphyrin deformation necessary for catalysis. The case for ferrochelatase may be similar to that of catalytic antibodies with ferrochelatase activity (*14*) for which certain amino acid residues appear to dominate the activation of the γ_{15} mode. Although residues of the loops in both the light chain and heavy chain contribute to mesoporphyrin deformation in the binding sites of the catalytic antibodies, mutational analysis indicates that the heavy chain dominates the γ_{15} mode activation (*14*). The dominant effect of porphyrin distortion in ferrochelatase is best illustrated by the K250M/V251L/W256Y variant, as it exhibits less than 30% of the γ_{15} mode activation (i.e., saddling) of the wild-type enzyme and very low activity. Thus, the traditional view of enzyme catalysis is epitomized by the ferrochelatase-catalyzed reaction that is mediated by the saddling deformation. Lowering of the transition state is driven by the enhanced binding energy of the strained substrate. The induced saddling occurs at the expense of weaker binding for the planar porphyrin in the active site, which favors the release of a metalated product since it more strongly prefers a planar conformation.

Consistent with the interpretation of the intensity of the activated γ_{15} mode as a measure of the degree of porphyrin distortion, Venkateshrao et al. (*14*) recently reported that the binding of mesoporphyrin IX to the Fab fragment of a ferrochelatase antibody (i.e., affinity-matured 7G12 antibody) promoted the activation of the γ_{15} Raman band at 680 cm^{-1}. The intensity of the induced Raman band was approximately 3-fold higher for this antibody than for the inactive germline

precursor antibody. Intermediate intensity values were observed for variants in which some of the residues where the somatic mutations had accumulated were mutated back to the germline residues (*14*). Significantly, a trend similar to what we observe for ferrochelatase and its variants was also identified with the catalytic efficiencies of the different catalytic antibodies. Indeed, an approximate linear correlation between the logarithm of the catalytic efficiencies and the γ_{15}/ν_7 intensity ratio could be established (*14*). From these results, the investigators concluded that γ_{15} activation was mainly proportional to the activation energy, reiterating the idea that catalysis involves straining of the substrate and that the active-site binding energy is evolved to lower the activation energy of the reaction (*14*).

We have observed a similar trend in the relationship between γ_{15} intensity and catalytic efficiency, but large experimental uncertainties and few data points do not reveal a true correlation. However, the data are suggestive, and they are consistent with other results obtained from quantum mechanical and molecular mechanics calculations, which indicated that the binding of a distorted porphyrin, particularly a saddled porphyrin, was thermodynamically preferred to that of a less flexible, metalated porphyrin (*15*). These results accentuate the importance of an architecture of the active site that binds a distorted porphyrin and releases a flatter, metalated porphyrin (*15*). Collectively, these studies of the loop variants and wild-type ferrochelatase indicate that a reduced level of saddling is associated with a decrease in catalytic efficiency (k_{cat}/K_m^{PP}) and an increase in K_m^{PP} (Table 1 and ref *18*), suggesting that the nonplanar conformation of the porphyrin substrate is favored in the interaction with the active site during the catalytic reaction. Studies involving synthetic nonplanar porphyrins in solvents of different polarity also have suggested that saddling affects the potential energy surfaces to allow porphyrin to access multiple configurations with small energy barriers from the ground state (*26*). A similar mechanism may be used in the protein matrix to solvate the porphyrin substrate and to facilitate its conversion into catalytically competent conformations. In this regard, it is probable that the saddled structure represents the ground state of the porphyrin−protein complex. Additionally, a saddled conformation may also serve to orient the substrate relative to the metal-binding site, since the reduced symmetry of the macrocyle might facilitate catalysis by promoting the proper alignment of porphyrin.

Active-Site Porphyrin-Binding Loop and Porphyrin Distortion. This RR examination of the conformation of metalloporphyrins (NiPP and hemin) and the natural porphyrin substrate (H_2PP) bound to the loop variants indicated that the loop residues, particularly the conserved tryptophan residue (W256 in murine ferrochelatase), induce porphyrin saddling. The degree of distortion was lowest in the K250M/V251L/W256Y variant, which also exhibited the lowest k_{cat} and the highest k_{cat}/K_m^{PP} values. Previously, we demonstrated that functional substitutions at the W256 position were very limited, whereas K250 and V251 tolerated multiple replacements and thus were less likely to play a critical role in porphyrin interaction (*18*). Significantly, independent, single mutations of W256 to Y, F, or R yield proteins of poor stability, which cannot be purified with the current available methods. Although the possibility that K250, V251, and W256 act synergistically to promote the strain of the porphyrin substrate cannot be dismissed, it is unlikely that K250 and V251 are the major determinants in porphyrin distortion for several reasons. First, in the structural model of murine ferrochelatase, the side chain of K250 is oriented toward the protein exterior (*18*), thus making it very unlikely that K250 would contact the bound porphyrin directly. Although the side chain of V251 is oriented toward the interior of the active-site cleft, the RR spectra of the V251L single mutant with bound porphyrin resemble those of the wild-type ferrochelatase (data not shown), indicating that the V251L mutation alone does not alter the degree of porphyrin distortion from that observed for the wild-type enzyme. Second, substitutions of K250 and V251 also occur in S249A/K250Q/V251C and Q248P/S249G/K250P/G252W variants with only a mild decrease in the level of porphyrin saddling, and in fact, these variants exhibited 80−85% of the wild-type extent of activation of the porphyrin distortion (Table 1). Third, the invariant W256 has its bulky aromatic side group oriented toward the interior of the active-site pocket. Finally, the role of steric interaction in macrocycle distortion was elucidated for the X-ray crystal structure of *B. subtilis* ferrochelatase with bound *N*-methylmesoporphyrin, a competitive inhibitor of ferrochelatase (PDB entry 1C1H) (*5*). Analysis of the crystallographic structure indicated that W230, equivalent to the murine W256 residue, lies in the proximity of the bound porphyrin (*5*). In particular, the minimum distance from C_6 of the tryptophan side chain to the nitrogen of pyrrole ring C of porphyrin is ca. 3 Å (Figure 5). Thus, the indole ring of the tryptophan residue is well-positioned to tilt the pyrrole group down, in the manner required to produce the observed saddling. In addition, the methyl group connected to the nitrogen atom of the opposite pyrrole ring (i.e., ring A) also acts to tilt down this pyrrole. Together, these factors contribute to the strong saddling observed in the crystal structure of ferrochelatase complexed with either *N*-methylmesoporphyrin or Cu(II) mesoporphyrin. In conclusion, although a synergistic effect may exist in the K250M/V251L/W256Y variant, the W256Y substitution would make it difficult for the side group to reach the proximal pyrrole ring and tilt it down, since tyrosine presents a phenolic ring shorter than the indole ring in tryptophan. Thus, substitution of W256 with the less bulky tyrosine would be expected to weaken the porphyrin distortion. The results of this RR study agree with the previous interpretation of the crystallographic structure of the *B. subtilis* ferrochelatase−*N*-methylmesoporphyrin complex, suggesting that, in the active site, aromatic stacking of the indole ring of Trp with a pyrrole ring of porphyrin is important in generating nonplanarity.

Other Structural Changes upon Porphyrin Binding. In addition to modulating the saddling of the porphyrin core, the mutations introduced into the active-site loop disrupt the interaction between the porphyrin vinyl groups and ferrochelatase, as indicated by the shifts and intensity changes of the vinyl-related RR lines. For H_2PP, the $\nu_{Ca=Cb}$ vinyl stretching band was sharpened upon protein binding (Figure 2B), suggesting that the vinyl groups had less freedom of movement and restricted orientation within the protein matrix. However, the vinyl lines of H_2PP bound to the variant K250M/V251L/W256Y appear to be less defined than in the spectra of the wild-type protein and the other variants.

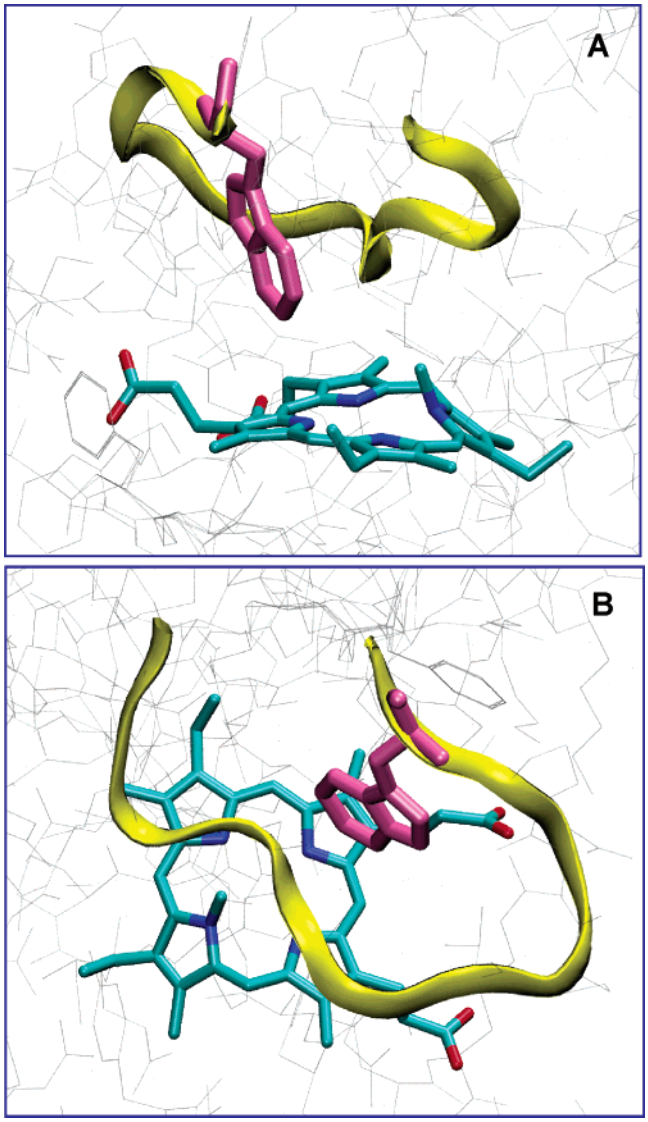

FIGURE 5: Three-dimensional views of the interaction between the invariant tryptophan residue and the active-site-bound porphyrin using the crystallized complex of *B. subtilis* ferrochelatase and *N*-MMP (PDB entry 1C1H) as a model structure. The bacterial W230 (purple) in the conserved loop motif (yellow) is shown to contact pyrrole ring C of the bound porphyrin macrocycle (cyan). The methyl group of *N*-MMP is attached to pyrrole ring A. When viewed from the top, pyrrole rings A−D of the porphyrin macrocycle are arranged in a clockwise manner in panels A and B.

Specifically, H_2PP bound to K250M/V251L/W256Y shows a broadening and downshift of the $\nu_{Ca=Cb}$ band and an upshift of ν_2, a vinyl-sensitive macrocycle vibration (Figure 2B, spectrum c), relative to those of the wild-type protein. A downshift of the $\nu_{Ca=Cb}$ vinyl stretching mode indicates rotation of the vinyl side chains into the plane of the porphyrin core, and broadening of the band suggests that the vinyl groups may have more motional freedom or adopt multiple alternative conformations (*27*, *28*). Thus, it is likely that the loop mutations cause more global changes in the active-site structure, which result in weakened interaction of the vinyl substituents with the protein matrix. Curiously, the restrictions on the vinyl substituents imposed by the protein are not unique to ferrochelatase, since catalytic antibodies with ferrochelatase activity catalyze insertion of metal into mesoporphyrin, which has ethyl groups in place of the vinyl groups in protoporphyrin, but not insertion of metal into the physiological substrate protoporphyrin IX (*12*).

Additional support for the idea that ferrochelatase can function to orient the vinyl groups comes from the enhancement of the $\nu_{Ca=Cb}$ vinyl stretching band of NiPP upon binding to ferrochelatase and loop variants (Figure 3B). There are also important changes in the vinyl-related lines of hemin bound to the P255R and P255G variants; specifically, the vinyl-related line ν_{38} intensifies (Figure 4B, spectra d and e). The mutations introduced into the porphyrin-binding loop appear to alter the global structure of the active site and consequently control the porphyrin ring that can be accommodated. Using ν_2 as a core-size marker (*29*), hemin shows an expansion of the core of the porphyrin ring when bound to the wild-type protein (Figure 4). A downshift of ν_2 for hemin bound to P255R and P255G implies that the ring is further expanded when compared to the wild-type ferrochelatase. The upshift of ν_2 in the K250M/V251L/W256Y, S249A/K250Q/V251C, and Q248P/S249G/K250P/G252W variants indicates that the ring core is less expanded than in the wild-type protein; similarly for NiPP, ν_2 and ν_{10} downshifted upon binding to the variant proteins (Figure 3B), suggesting that the core of the ring was similarly enlarged in the protein environment of the wild-type ferrochelatase and variants. While unbound NiPP adopts both planar and nonplanar conformations in solution, as shown by the deconvolution of the asymmetric ν_{10} band into planar and nonplanar components, only a nonplanar form is observed in the mutated protein environment (*16*).

Structural changes other than saddling are evident in the RR spectra. Although ν_2, ν_3, and ν_{10} of NiPP exhibited downshifts suggestive of the same overall porphyrin in-plane distortion for the wild-type and all the ferrochelatase variants, the assayed variants did not exhibit line shifts in the low-frequency region of the RR spectra as extensive as those observed for the wild-type ferrochelatase (Figure 3). NiPP bound to the triple (K250M/V251L/W256Y and S249A/K250Q/V251C) and quadruple (Q248P/S249G/K250P/G252W) variants led to a less pronounced splitting of the two lines near the position of ν_7 (Figure 3A). In addition, the relative intensity of the propionate lines near 375 nm changes less upon binding to wild-type ferrochelatase than for these variants. Finally, the line including ν_8, a line known to be sensitive to macrocycle and substituent conformations, exhibits a spectral shape for these variants that is more similar to that observed for the porphyrin free in solution than that for the wild-type bound species. These results are all indicative of a looser and less specific interaction between NiPP and the active site of the triple and quadruple variants. Similar features are observed (Figure 4) when these variants are incubated with hemin, an inhibitor of the enzyme. For example, ν_7 did not exhibit any appreciable downshift as opposed to that of the wild-type protein−hemin complex, and ν_2 in the high-frequency spectral region appeared to be more like that of hemin in buffer than that of hemin bound to the wild-type protein. Overall, the NiPP and hemin RR results for the multiple variants are indicative of less specific binding to the protein and a less pronounced porphyrin distortion induced by these variants in comparison with wild-type ferrochelatase.

In conclusion, the conserved active-site loop motif in ferrochelatase plays an important role in porphyrin binding

and distortion. Most significantly, the induced porphyrin saddling is shown to modulate the catalytic efficiency of ferrochelatase toward its substrate, and the invariant tryptophan is a major protein determinant of the saddled conformation of the macrocycle. Additionally, the loop residues function in specifically orienting the porphyrin vinyl substituents and likely the entire porphyrin ring.

REFERENCES

1. Dailey, H. A., and Dailey, T. A. (2003) Ferrochelatase, in *The Porphyrin Handbook* (Kadish, K. M., Smith, K. M., and Guilard, R., Eds.) pp 93−121, Elsevier Science, New York.
2. Ferreira, G. C. (1999) Ferrochelatase, *Int. J. Biochem. Cell Biol. 31*, 995−1000.
3. Ferreira, G. C., Franco, R., Lloyd, S. G., Moura, I., Moura, J. J. G., and Huynh, B. H. (1995) Structure and function of ferrochelatase, *J. Bioenerg. Biomembr. 27*, 221−229.
4. Al-Karadaghi, S., Hansson, M., Nikonov, S., Jonsson, B., and Hederstedt, L. (1997) Crystal structure of ferrochelatase: The terminal enzyme in heme biosynthesis, *Structure 5*, 1501−1510.
5. Lecerof, D., Fodje, M., Hansson, A., Hansson, M., and Al-Karadaghi, S. (2000) Structural and mechanistic basis of porphyrin metallation by ferrochelatase, *J. Mol. Biol. 297*, 221−232.
6. Wu, C. K., Dailey, H. A., Rose, J. P., Burden, A., Sellers, V. M., and Wang, B. C. (2001) The 2.0 Å structure of human ferrochelatase, the terminal enzyme of heme biosynthesis, *Nat. Struct. Biol. 8*, 156−160.
7. Karlberg, T., Lecerof, D., Gora, M., Silvegren, G., Labbe-Bois, R., Hansson, M., and Al-Karadaghi, S. (2002) Metal binding to *Saccaromyces cerevisiae* ferrochelatase, *Biochemistry 41*, 13499−13506.
8. Lecerof, D., Fodje, M. N., Alvarez, L. R., Olsson, U., Hansson, A., Sigfridsson, E., Ryde, U., Hansson, M., and Al-Karadaghi, S. (2003) Metal binding to *Bacillus subtilis* ferrochelatase and interaction between metal sites, *J. Biol. Inorg. Chem. 8*, 452−458.
9. Dailey, H. A. (1990) in *Biosynthesis of Heme and Chlorophylls* (Dailey, H. A., Ed.) pp 142−147, McGraw-Hill Book Co., New York.
10. Blackwood, M. E., Jr., Rush, T. S., Romesberg, F., Schultz, P. G., and Spiro, T. G. (1998) Alternative modes of substrate distortion in enzyme and antibody catalyzed ferrochelation reactions, *Biochemistry 37*, 779−782.
11. Blackwood, M. E., Rush, T. S., Medlock, A., Dailey, H. A., and Spiro, T. G. (1997) Resonance Raman spectra of ferrochelatase reveal porphyrin distortion upon metal binding, *J. Am. Chem. Soc. 119*, 12170−12174.
12. Cochran, A. G., and Schultz, P. G. (1990) Antibody-catalyzed porphyrin metallation, *Science 249*, 781−783.
13. Yin, J., Andryski, S. E., Beuscher, A. E., IV, Stevens, R. C., and Schultz, P. G. (2003) Structural evidence for substrate strain in antibody catalysis, *Proc. Natl. Acad. Sci. U.S.A. 100*, 856−861.
14. Venkateshrao, S., Yin, J., Jarzecki, A. A., Schultz, P. G., and Spiro, T. G. (2004) Porphyrin distortion during affinity maturation of a ferrochelatase antibody, monitored by Resonance Raman spectroscopy, *J. Am. Chem. Soc. 126*, 16361−16367.
15. Sigfridsson, E., and Ryde, U. (2003) The importance of porphyrin distortions for the ferrochelatase reaction, *J. Biol. Inorg. Chem. 8*, 272−282.
16. Franco, R., Ma, J. G., Lu, Y., Ferreira, G. C., and Shelnutt, J. A. (2000) Porphyrin interactions with wild-type and mutant mouse ferrochelatase, *Biochemistry 39*, 2517−2529.
17. Lu, Y., Sousa, A., Franco, R., Mangravita, A., Ferreira, G. C., Moura, I., and Shelnutt, J. A. (2002) Binding of Protoporphyrin IX and Metal Derivatives to the Active Site of Wild-Type Mouse Ferrochelatase at Low Porphyrin-to-Protein Ratios, *Biochemistry 41*, 8253−8262.
18. Shi, Z., and Ferreira, G. C. (2004) Probing the active site loop motif of murine ferrochelatase by random mutagenesis, *J. Biol. Chem. 279*, 19977−19986.
19. Ferreira, G. C. (1994) Mammalian ferrochelatase. Overexpression in *Escherichia coli* as a soluble protein, purification and characterization, *J. Biol. Chem. 269*, 4396−4400.
20. Laemmli, U. K. (1970) Cleavage of structural proteins during the assembly of the head of bacteriophage T4, *Nature 227*, 680−685.
21. Smith, P. K., Krohn, R. I., Hermanson, G. T., Mallia, A. K., Gartner, F. H., Provenzano, M. D., Fujimoto, E. K., Goeke, N. M., Olson, B. J., and Klenk, D. C. (1985) Measurement of protein using bicinchoninic acid, *Anal. Biochem. 150*, 76−85.
22. Shi, Z., and Ferreira, G. C. (2003) A continuous anaerobic fluorimetric assay for ferrochelatase by monitoring porphyrin disappearance, *Anal. Biochem. 318*, 18−24.
23. Dailey, H. A., and Fleming, J. E. (1983) Bovine ferrochelatase. Kinetic analysis of inhibition by *N*-methylprotoporphyrin, manganese, and heme, *J. Biol. Chem. 258*, 11453−11459.
24. Jarzecki, A. A., and Spiro, T. G. (2005) Porphyrin Distortion from Resonance Raman Intensities of Out-of-Plane Modes: Computation and Modeling of *N*-Methylmesoporphyrin, a Ferrochelatase Transition State Analog, *J. Phys. Chem. A 109*, 421−430.
25. Hu, S., Smith, K. M., and Spiro, T. G. (1996) Assignment of Protoheme Resonance Raman Spectrum by Heme Labeling in Myoglobin, *J. Am. Chem. Soc. 118*, 12638−12646.
26. Sazanovich, I. V., Galievsky, V. A., van Hoek, A., Schaafsma, T. J., Malinovskii, V. L., Holten, D., and Chirvony, V. S. (2001) Photophysical and Structural Properties of Saddle-Shaped Free Base Porphyrins: Evidence for an "Orthogonal" Dipole Moment, *J. Phys. Chem. B 105*, 7818−7829.
27. Marzocchi, M. P., and Smulevich, G. (2003) Relationship between heme vinyl conformation and the protein matrix in peroxidases, *J. Raman Spectrosc. 34*, 725−736.
28. Kalsbeck, W. A., Ghosh, A., Pandey, K. P., Smith, K. M., and Bocian, D. F. (1995) Determinants of the vinyl stretching frequency in protoporphyrins. Implications for cofactor-protein interactions in heme proteins, *J. Am. Chem. Soc. 117*, 10959−10968.
29. Parthasarathi, N., Hansen, C., Yamaguchi, S., and Spiro, T. G. (1987) Metalloporphyrin core size resonance Raman marker bands revisited: Implications for the interpretation of hemoglobin photoproduct Raman frequencies, *J. Am. Chem. Soc. 109*, 3865−3871.

BI051907I